Materials Characterization xxx (xxxx) xxx–xxx

Contents lists available at ScienceDirect

Materials Characterization

journal homepage: www.elsevier.com/locate/matchar

Selective growth of Ni_4Ti_3 precipitate variants induced by complicated cyclic stress during Laser additive manufacturing of NiTi-based composites

Chenglong Ma[a,b], Dongdong Gu[a,b,*], Donghua Dai[a,b], Mujian Xia[a,b], Hongyu Chen[a,b]

[a] College of Materials Science and Technology, Nanjing University of Aeronautics and Astronautics, Yudao Street 29, Nanjing 210016, PR China
[b] Jiangsu Provincial Engineering Laboratory for Laser Additive Manufacturing of High-Performance Metallic Components, Nanjing University of Aeronautics and Astronautics, Yudao Street 29, Nanjing 210016, PR China

ARTICLE INFO

Keywords:
Selective laser melting (SLM)
NiTi shape memory alloy
Ni_4Ti_3 precipitate

ABSTRACT

NiTi-based composites were in-situ synthesized by selective laser melting (SLM) additive manufacturing technology with formation of a great many Ni_4Ti_3 precipitates. The differential scanning calorimetry (DSC) were carried out to exhibit the similar phase transformation temperature (A_s = 51.82 °C, A_f = 94.02 °C, M_s = 55.87 °C and M_f = 18.93 °C) by comparing with that of SLM-fabricated equi-atomic NiTi alloy, which could be attributed to the compensation of Ni_4Ti_3 precipitates for the effect of an addition of TiC particles. Three different Ni_4Ti_3 precipitate variants ($(111)_R//(1\bar{1}\bar{1})_{B2}$, $(111)_R//(\bar{1}\bar{1}1)_{B2}$, and $(111)_R//(\bar{1}1\bar{1})_{B2}$) with various precipitate diameters were observed within SLM fabricated part, showing apparently selective growth behavior. By high-resolution transmission electron microscopy, severe lattice defects formed surrounding the smaller variant, while relatively intact lattice structure was found around the larger one, which indicated that high strain energy was produced in the interface between the matrix and the smaller variant. Furthermore, finite element simulation method was applied to disclose the evolution features of complicated cyclic stress during SLM processing of TiC/NiTi composites. By predicting, the main constraint mode within as-fabricated track was tensile stress effect. Based on the redistribution behavior of thermal stress and the coupling effect between the thermal stress and strain field induced by Ni_4Ti_3 precipitate, the selective growth mechanism of Ni_4Ti_3 variant was revealed.

1. Introduction

NiTi-based alloys have attracted most attention due to their unique shape memory effect (SME) found by Buehler et al. in 1963 and the superelasticity (SE), and meanwhile entered a wide range of engineering applications from medical implants to actuators, inflatable structures and shock-absorbing structures, etc. [1–4]. Note that, both SME and SE are attributed to a reversible austenite-martensite phase transformation, which are induced by temperature change and applied stress, respectively [5,6]. Specially, as two crucial characteristic indexes for the functionality natures of NiTi-based alloys, the martensitic transformation temperature (M_s) and path (B2–B19′ or B2-R-B19′) are usually required to get tailored according to different application conditions. A considerable number of investigations have confirmed that strong coupling exists between Ni_4Ti_3 precipitate and martensitic transformations [7–9]. Hence, the SME or SE is usually controlled by the existence of Ni_4Ti_3 precipitates in the Ni-rich NiTi-based alloys [10]. With regard to Ni_4Ti_3 precipitate, it has eight variants falling into four {111}-plane groups (PGs), which meant that the central disk $(111)_R$ of Ni_4Ti_3 precipitates with various variants are respectively parallel to one of $\{111\}_{B2}$ families of planes of the NiTi matrix (namely $(1\bar{1}\bar{1})_{B2}$, $(\bar{1}1\bar{1})_{B2}$, $(\bar{1}\bar{1}1)_{B2}$ and $(111)_{B2}$) [11]. And it was found that Ni_4Ti_3 precipitates with only one type variant could lead to an excellent two-way SME [12].

Recently, the combination of the prevailing laser additive manufacturing (LAM, mainly containing selective laser melting (SLM) and laser melting deposition (LMD)) technology and NiTi shape memory alloys has further expanded the concept of 3D printing to 4D printing [13,14]. Note that, M. Elahinia et al. from the University of Toledo have carried out a great many works, devoting themselves to showing how the LAM process influences structural and functional properties of laser additive manufactured Ni-Ti alloys [2,15–18]. Besides, they further studied the influence of heat treatment on thermomechanical response of laser additive manufactured Ni-Ti alloys [19,20]. However, to the best of our knowledge, few attentions have been focused on the precipitation of Ni_4Ti_3 intermetallic during LAM processing NiTi-based alloys, except the following work. Beth A. Bimber et al. studied the anisotropic microstructure and superelasticity of LMD-processed Ni-rich NiTi alloy, finding that the Ni_4Ti_3 precipitate as a predominant microconstituent existed and the stress-induced martensitic phase

* Corresponding author at: College of Materials Science and Technology, Nanjing University of Aeronautics and Astronautics, Yudao Street 29, Nanjing 210016, PR China.
E-mail address: dongdonggu@nuaa.edu.cn (D. Gu).

https://doi.org/10.1016/j.matchar.2018.04.004
Received 27 October 2017; Received in revised form 25 March 2018; Accepted 3 April 2018
1044-5803/

transformation predominately occurred in the region with finer precipitate morphology [21]. It indicated that by controlling the size and distribution of Ni_4Ti_3 precipitates, the tailored M_s and transformation path could be obtained. In fact, during LAM, the thermal cycle nature determined by track-by-track and layer-by-layer processing manner results in the complexity and dissimilarity of thermodynamics behavior and thermal-stress coupling behavior within different laser melting elements [22], which poses a great challenge to control the size, distribution and variant type of Ni_4Ti_3 precipitates. Hence, at present, it is urgent to reveal the inherent influence mechanism of thermal/stress nature on the precipitate/growth behavior of Ni_4Ti_3 during LAM, and to master the corresponding control methods.

In our latest work [23], we have attempted the SLM of the Ni-Ti-TiC material system. As for the introduction of TiC, on one hand, TiC particle can significantly enhance the mechanical properties such as wear resistance, strength, stiffness and hardness, of NiTi alloy [24]. For another thing, R.Vaidyanathan et al. suggested that the mechanical deformation behavior of TiC/NiTi composites was both of theoretical interest (to better understand deformation mechanisms, e.g. twinning or stress-induced transformations) and practical interest (as superelastic composites) [25]. Interestingly, during SLM of Ni-Ti-TiC blended powder (Ti-rich material system), complicated heat and mass transfer tended to cause the formation of non-stoichiometric TiC_x, further leading to precipitation of a nickel-rich intermetallic Ni_4Ti_3 within the matrix. In that work, we mainly focused on the in-situ formation of Ni_4Ti_3 precipitates and their effect on the pseudoelastic recovery of the fabricated part. Turn to this paper, we more concerned about the variant type and growth of Ni_4Ti_3 precipitates. Specially, the distribution feature of complicated thermal behavior induced cyclic stress and its effect on growth behavior of different Ni_4Ti_3 variants during LAM processing of NiTi-based composites were elaborated.

2. Materials, Experimental Procedure and Characterization Method

The spherical Titanium powder and Nickel powder as well as the irregular-shaped TiC particle were used as the raw materials in this study. The mean particle size of Titanium powder, Nickel powder and TiC particle were 25 μm, 10 μm and 6 μm, respectively. Then the multi-powders consisting of 40 wt% Titanium powder, 50 wt% Nickel powder and 10 wt% TiC particle were homogenously mixed for SLM processing which was performed by the SLM-150 equipment developed by Nanjing University of Aeronautics and Astronautics. Details concerning the applied mixing equipment, SLM equipment and processing procedures have been addressed in literature [26]. By the parameter optimization, the following suitable processing parameters were chosen: the laser power of 110 W, the scan speed of 200 mm/s, and the powder layer thickness of 30 μm were settled. A simple linear raster scan pattern was used with a hatch spacing of 50 μm. By SLM consolidation procedure, the box-shaped specimens with the dimensions of 9 mm × 9 mm × 5 mm were fabricated.

The transmission electron microscope (TEM) and high resolution TEM (HRTEM) were carried out by using a Tecnai G2 F20 S-TWIN (200KV) (FEI. co., the USA) in this study. The Thermo Scientific™ ARL™ X'TRA X-ray diffractometer (XRD) with Cu Kα radiation (λ = 0.154 18 nm) using a continuous scan mode was applied to identify the phases of the SLM-fabricated specimens within a narrow range of 2θ = 30–80°. The phase transformation temperature of SLM-fabricated composites was revealed by using Pyris 1 DSC (PerKinElmer, USA) differential scanning calorimetry (DSC) with a heating and cooling rate of 20 °C/min from 0 °C to 120 °C.

3. Finite Element Modeling for Thermal-Stress Coupling Behavior

Furthermore, to give more insight into growth behavior of Ni_4Ti_3 precipitates with different variants during SLM processing, a three-dimensional stress field modeling of TiC/NiTi composites based on finite element method was established. To simplify the model, the powder bed is considered to be isotropic and continuous material. Meanwhile, the thermal physical parameters including the thermal conductivity, the constant pressure special heat capacity, elasticity modulus and coefficient of thermal expansion of TiC/NiTi composites were estimated by the weighted average method. Note that, the physical model description, thermal modeling, boundary conditions and heat source modeling of TiC/NiTi composites in this paper are consistent with that in our previous simulation work on residual stresses in SLM-processed Ti-Ni shape memory alloy [27]. Hence, the specific description on this model was not repeated here. Subsequently, the birth-death element arithmetic and thermal-stress coupling method were introduced into simulating stress evolution and distribution of SLM-processed TiC/NiTi composites single layer with multi-tracks. The coupling relationship between the localized temperature and the corresponding thermal stress/strain can be described as follows [28]:

$$\{\varepsilon\} = [D]^{-1}\{\sigma\} + \alpha_{CTE} \times (T - T_{ref}) \quad (1)$$

in which $\{\varepsilon\}$ is total strain, $[D]$ is stress-strain matrix, $\{\sigma\}$ is stress matrix, T is the operating temperature and T_{ref} is reference temperature.

4. Results and Discussion

4.1. Phase Transformation Behavior

Fig.1 (a) exhibits the XRD pattern of SLM-processed Ni-Ti-C composites. The B2 (NiTi) phase was clearly identified by XRD with the strongest main diffraction peak corresponding to (110) $_{B2}$ and the relatively weaker diffraction peak corresponding to (211) $_{B2}$. Besides, Ni-rich Ni_4Ti_3 and non-stoichiometric $Ti_6C_{3.75}$ phase was also detected. Subsequently, the DSC test was performed to obtain the heat flow-temperature curves of SLM-processed Ni-Ti-C composites during the heating and cooling (Fig. 1 (b)). Exothermic peak and endothermic peak were clearly observed in a temperature range of 0–100 °C, which indicated that a reversible solid-state phase transformation occurred during heating-cooling cycle process. According to the detected phases, it was reasonable to believe that the martensite phase was transformed to austenite phase during heating, while austenite-to-martensite phase transformation occurred during cooling process, further verifying the in-situ formation of NiTi phase with the capacity of shape memory effect. Specially, another small peak near the apparent main peak from the DSC curve could be found, the first one of which was often attributed to the existence of Ni-rich precipitates [2]. In this study, the measured A_s (martensite-to-austenite transformation start temperature), A_f (martensite-to-austenite transformation finish temperature), M_s (austenite-to-martensite transformation start temperature) and M_f (austenite-to-martensite transformation finish temperature) respectively reached 51.82 °C, 94.02 °C, 55.87 °C and 18.93 °C. Meanwhile, it was not difficult to see that the exothermic and endothermic energy (ΔH_{ex} = 1.1634 J/g and ΔH_{en} = −0.5098 J/g) were limited.

Haberland et al. had compared the transformation temperature of three different material composition of SLM fabricated NiTi corresponding to the Ni-rich, the equi-atomic and the Ti-rich [2]. They found the transformation temperature tended to rise with the Ni content of Ni-Ti alloy decreasing and the equi-atomic one showed the A_s = 325 K and M_s = 327 K which were very close to our measured results of SLM fabricated TiC/NiTi composites. For the TiC/NiTi material system, D. Mari and D. C. Dunand had showed that addition of TiC particles could affect the transformation temperatures and lower both the A_s and M_f due to the transformation misfit stresses [29]. Hence, it could be speculated that the existence of Ni_4Ti_3 precipitates mostly compensated the effect of TiC particles on transformation temperatures of the matrix, in consideration of formation of a depletion of nickel as Ni_4Ti_3 precipitated.

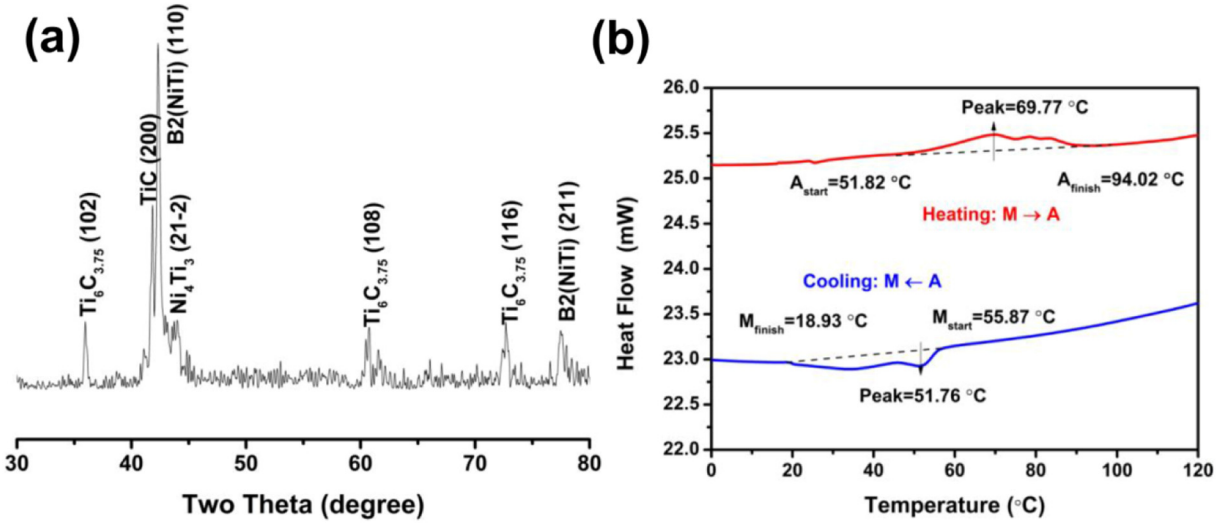

Fig. 1. (a) the XRD pattern of SLM fabricated Ni-Ti-C composites with 30–80°; (b) the DSC curve detected from 0 °C to 120 °C.

4.2. Different Ni_4Ti_3 Precipitate Variants

Fig. 2 gives the detailed structure morphology of grey lenticular Ni_4Ti_3 precipitates with various precipitate diameters formed during SLM processing. The long axis of Ni_4Ti_3 precipitates displayed three different orientations (Fig. 2(a) and (b)) and the corresponding schematic was shown in Fig. 2(c). The angle between any two of these precipitates with different orientations was approximately 60° by measuring. The corresponding selected area diffraction pattern (SADP) was conducted, from which the B2 and Ni_4Ti_3 phases were identified clearly (Fig. 2(d) and (e)). Three different types of diffraction spot arrays were distinguished, respectively corresponding to the three different Ni_4Ti_3 precipitate variants. Besides, strong diffraction spots corresponding to B2 (NiTi) were detected with the main planes of (110) $_{B2}$, (101) $_{B2}$, and (211) $_{B2}$ for regions B and C, according to which $[1\bar{1}\bar{1}]_{B2}$ zone axis could be achieved. The orientation relationship between the B2 cubic structure and the Ni_4Ti_3 ellipsoids belonging to different PGs was illustrated in Fig. 2 (f). When viewing along $[1\bar{1}\bar{1}]_{B2}$ zone axis, structure morphology of all variants demonstrated the lenticular shape, orientation relationship of long axis of which was consistent with the

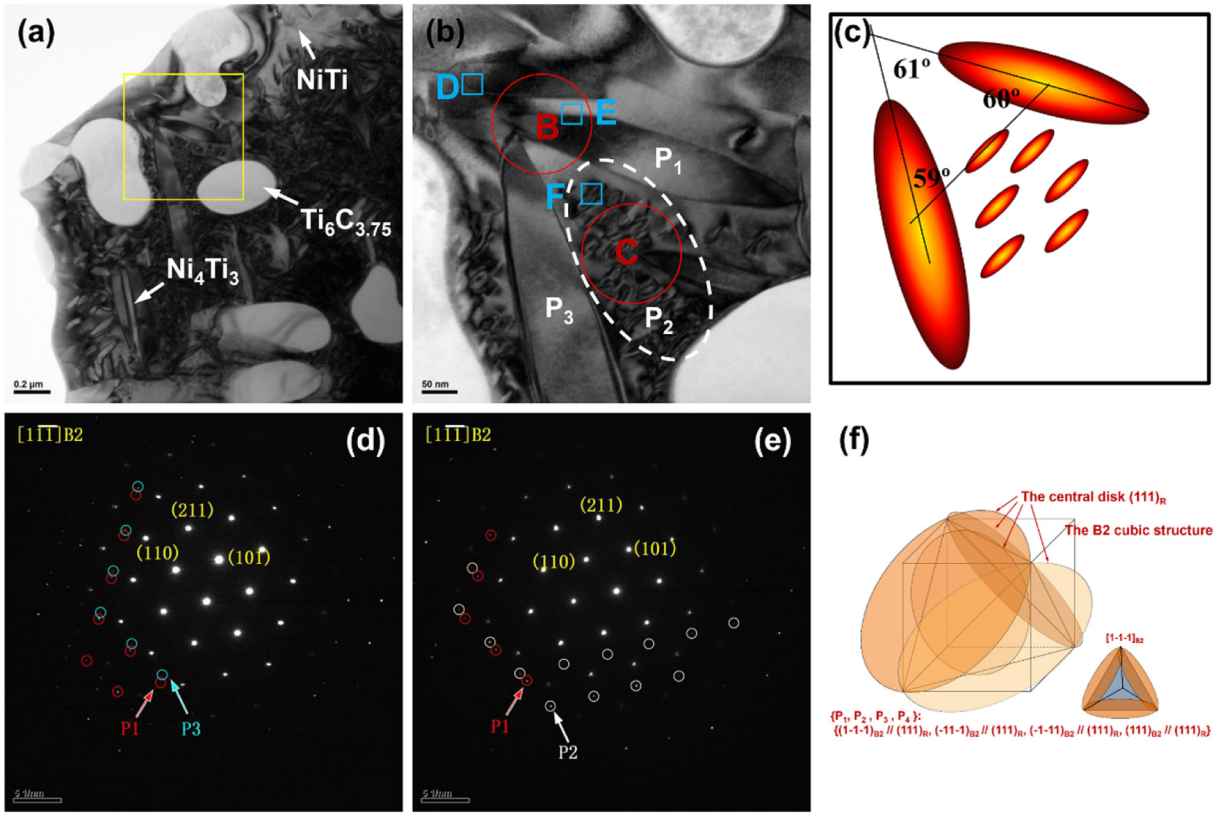

Fig. 2. (a) the fine structure of Ni_4Ti_3 precipitate; (b) the local high-magnification image of (a); (c) the orientation relationship of Ni_4Ti_3 precipitates with various variants; (d) and (e) SADPs respectively corresponding to the region B and C in (b); (f) the schematic of the Ni_4Ti_3 ellipsoids belonging to different PGs. (For interpretation of the references to color in this figure, the reader is referred to the online version of this chapter.)

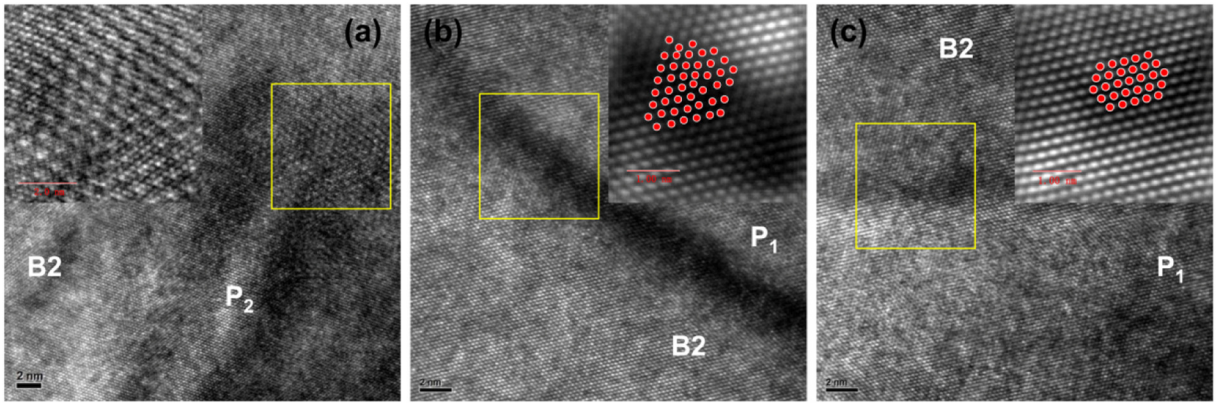

Fig. 3. (a) HRTEM image of the interface between P_2-type variant and the matrix corresponding to zone D in Fig. 2 (b); HRTEM images of the interface between P_1-type variant and the matrix (b) corresponding to zone E in Fig. 2 (b) as well as (c) corresponding to zone F in Fig. 2 (b).

observed results (Fig. 2(b)), as shown in the lower right corner of Fig. 2(f). For the sake of clarity, the various Ni_4Ti_3 variants were numbered as P_1, P_2, P_3, and P_4, and P_4 stand for the variant with $(111)_{Ni_4Ti_3}//(1\bar{1}\bar{1})_{B2}$ by assuming. Meanwhile, three different Ni_4Ti_3 variants viewed in Fig. 2 (b) tentatively respectively belonged to P_1, P_2 and P_3. It was worthy to be paid attentions to the difference in the precipitate diameter (precipitate diameter of P_2-type Ni_4Ti_3 was only 20–30 nm, far smaller than that of P_1-type and P_3-type). The HRTEM images of the particle edge of Ni_4Ti_3 with different precipitate diameters, corresponding to region D, region E and region F (as the blue pane shown in Fig. 2 (b)) were present in Fig. 3. And meanwhile, the reverse Fourier transformation was applied to exhibit the lattice structure of the precipitate-matrix interface. For the small P_2-type Ni_4Ti_3, a great many lattice defects (including point defects, lattice distortion, etc.) were found near the interface showing high strain energy which to some extent accounted for growth restriction (Fig. 3 (a)), while interface structure with relatively well coherent relationship was clearly observed for P_1-type (Fig. 3 (b) and (c)). Besides, for the same P_1-type variant, apparent lattice defects were also found to exist within one with the smaller size (Fig. 3 (b)).

D. Y. Li et al. indicated that this selective growth behavior of Ni_4Ti_3 variant could be attributed to inner or ex-stress constraint effect [30]. They found the Ni_4Ti_3 variant which was nearly perpendicular to the *x*-axis grew preferentially while the other variant was retarded under a compressive strain-constraint, and the opposite effect was got under a tensile strain-constraint [31]. In fact, during SLM processing, the cyclic thermal stress induced by complicated thermal behaviors was considerable, which was believed to be responsible for an anisotropic distribution of precipitate variants. The detailed interpretations were carried out in the next section.

4.3. Stress Distribution and its Effect on Growth of Different Ni_4Ti_3 Variants

Fig. 4 depicts the stress distribution of adjacent three scanning tracks during the track-by-track manufacturing of SLM, being predicted by finite element simulation of thermal-stress coupling model. It was not hard to see that the main constraint mode of as-fabricated track was tensile stress effect during SLM processing. Heterogeneous stress distribution was apparent as the laser beam moved over powder bed, according to the stress field cloud pictures (Fig. 4 (a)–(c)). Simultaneously, stress behavior of the being fabricated track could result in redistribution of residual stress within the previous several tracks. Fig. 4 (d)–(f) respectively shows stress-time evolution curve of the central point of each track (first track, second track and third track). As the first track was fabricated, X-component stress was the predominant stress behavior, taking account of the lower value of Y-component and *Z*-component stress (Fig. 4 (d)). That meant the direction of stress was mainly parallel to the scanning direction in this condition. Nevertheless, both X-component and Y-component stress became the main stress component, when the laser beam moved to the second track and the third track (Fig. 4 (d)).

The formation of complicated thermal stress field during SLM played a crucial role in growth of Ni_4Ti_3 precipitates with different variants. According to the calculation of D. Y. Li et al. [30], the critical angle β between the applied stress and $[111]_{B2}$ was 51° at which the coupling strain energy $-\sigma_{kl}{}^{a}\varepsilon_{kl}{}^{0}V_p$ determining the selective growth of variant with $(111)_R//(111)_{B2}$ was equal to zero. Here, $\sigma_{kl}{}^{a}$was the applied stress, $\varepsilon_{kl}{}^{0}$was the eigenstrain and $V_p$was the volume of Ni_4Ti_3 precipitates. When the measured angle was higher 51°, the applied tensile stress could reduce the strain energy and consequently favor the growth of the precipitate variant, while the compressive stress retarded the growth. In the views of the high symmetry of B2 structure, the critical angle was considered as 51° here for the other variants. Besides, it is well acknowledged that the preferential orientation for growth of B2 matrix is $\langle 111\rangle_{B2}$, parallel to the heat flow direction within the molten pool. At the top region of molten pool, the preferential orientation was parallel to the direction of stress based on the above discussion, as the first track was fabricated (Fig. 4 (g)). Here, giving that the preferential orientation for growth of B2 matrix was $[1\bar{1}\bar{1}]_{B2}$. Then the angle among the normal direction of crystal face of $(111)_{B2}$, $(\bar{1}1\bar{1})_{B2}$ and $(\bar{1}\bar{1}1)_{B2}$ and $[1\bar{1}\bar{1}]_{B2}$ was 70.53°. As a result, growth of variant with $(111)_R//(1\bar{1}\bar{1})_{B2}$ got restricted and the other ones grew preferentially (Fig. 4 (h)). With the laser beam moving to next track, redistribution of stress within the first track occurred. In this case, direction of Y-component stress was parallel to $(1\bar{1}\bar{1})_{B2}$, which might as well be parallel to $[211]_{B2}$ here by assuming. Thus, the calculated angle respectively reached 90°, 19.47°, 61.87° and 61.87°, corresponding to variant with $(111)_R//(1\bar{1}\bar{1})_{B2}$, $(111)_R//(111)_{B2}$, $(111)_R//(\bar{1}\bar{1}1)_{B2}$, and $(111)_R//(\bar{1}1\bar{1})_{B2}$. Only growth of variant with $(111)_R//(111)_{B2}$ got remarkably retarded. Taking account of effect of X-component stress, variants with $(111)_R//(\bar{1}\bar{1}1)_{B2}$ and $(111)_R//(\bar{1}1\bar{1})_{B2}$ grew sufficiently, while growth of variants with $(111)_R//(111)_{B2}$ and $(111)_R//(1\bar{1}\bar{1})_{B2}$ was limited to some degree (Fig. 4 (i)), which was consistent with the observed results (Fig. 2b). The similar redistribution behavior of stress took place in the next tracks as the laser beam moving successively, therefore leading to morphology evolution of different Ni_4Ti_3 variants within next track. Taking into account of pre-heating effect from the previous fabricated track, value of inner stress within the being fabricated track decreased significantly (Fig. 4 (e) and (f)). Consequently, stress-induced effect got weakened, thus suppressing the growth of all existed Ni_4Ti_3 variants and precipitation of Ni_4Ti_3 phase in the previous track induced by self-aging treatment [23] and accounting for the difference in precipitate size for the same variant. Note that, stress behavior within SLM fabricated component can be tailored by changing laser processing

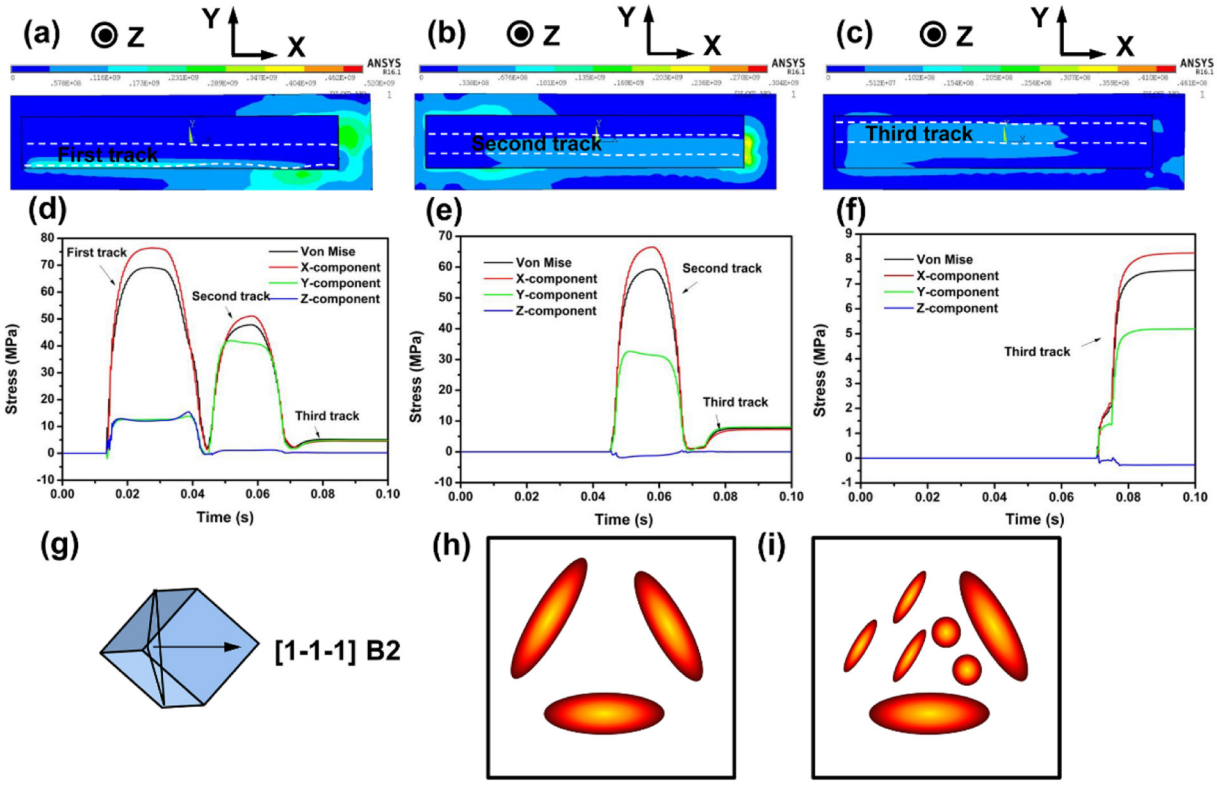

Fig. 4. (a)–(c) the stress distribution cloud pictures respectively corresponding to the first track, the second track and the third track; the stress-time curves of the central points of (d) the first track, (e) the second track and (f) the third track; (g) the cubic structure of B2 matrix; (h) growth of Ni_4Ti_3 variants only when the first track was fabricated; (i) growth of Ni_4Ti_3 variants as the second track was fabricated.

parameters including laser power, scan speed and scan strategy, etc [28]. Hence, it was accordingly possible to achieve the tailored microstructure with as-designed Ni_4Ti_3 variant.

5. Conclusions

In this work, NiTi-based composites were in-situ prepared by SLM of the raw Ti, Ni, and TiC blended powder. The following main conclusions could be drawn, based on the results and analysis in this paper:

(1) The exothermic peak and the endothermic peak respectively corresponding to heating and cooling process were detected clearly by DSC. The phase transformation temperatures were measure as A_s = 51.82 °C, A_f = 94.02 °C, M_s = 55.87 °C and M_f = 18.93 °C. By comparing with Haberland et al.'s work [2], the results were similar as that of the SLM-fabricated equi-atomic NiTi alloy, which could be attributed to the combination effect of an addition of TiC particles and in-situ precipitation of Ni_4Ti_3.

(2) Three different typical lenticular Ni_4Ti_3 variants including variant with $(111)_R//(1\bar{1}\bar{1})_{B2}$,$(111)_R//(\bar{1}\bar{1}1)_{B2}$, and $(111)_R//(\bar{1}1\bar{1})_{B2}$ were found by the characterization of TEM and SADP. Note that, precipitate diameters of these three Ni_4Ti_3 variants varied, showing the apparent selective growth feature. Higher lattice strain energy formed in the interface between the smaller Ni_4Ti_3 variant and the matrix.

(3) Thermal-stress coupling modeling of SLM-fabricated TiC/NiTi composites was established. As the laser moved successively from the first track to the third track, the residual stress direction of the starting side of the first track varied due to the change of the main stress component, which further accounted for selective growth behavior of Ni_4Ti_3 variant at this position.

Acknowledgements

We are grateful for the financial support from the National Natural Science Foundation of China (Nos. 51575267); the National Key Research and Development Program “Additive Manufacturing and Laser Manufacturing” (No. 2016YFB1100101); the NSFC-DFG Sino-German Research Project (No. GZ 1217), the Key Research and Development Program of Jiangsu Provincial Department of Science and Technology of China (No. BE2016181); the Aeronautical Science Foundation of China (No. 2015ZE52051); the Top-Notch Young Talents Program of China; and the Priority Academic Program Development of Jiangsu Higher Education Institutions. One of authors thanks the financial support from the Funding for Outstanding Doctoral Dissertation in NUAA (No. BCXJ17-05) and Postgraduate Research & Practice Innovation Program of Jiangsu Province (No. KYCX17-0253).

References

[1] G. Tadayyon, M. Mazinani, Y. Guo, S.M. Zebarjad, S.A.M. Tofail, M.J.P. Biggs, Mater. Charact. 112 (2016) 11–19.
[2] C. Haberland, M. Elahinia, J.M. Walker, H. Meier, J. Frenzel, Smart Mater. Struct. 23 (2014) 104002.
[3] K. Otsuka, X. Ren, Prog. Mater. Sci. 50 (2005) 511–678.
[4] S. Dadbakhsh, M. Speirs, J.V. Humbeeck, J.-P. Kruth, MRS Bull. 41 (2016) 765–774.
[5] W. Tirry, D. Schryvers, K. Jorissen, D. Lamoen, Acta Crystallogr. B 62 (2006) 966–971.
[6] S. Li, H. Hassanin, M.M. Attallah, N.J.E. Adkins, K. Essa, Acta Mater. 105 (2016) 75–83.
[7] N. Zhou, C. Shen, M.F.–.X. Wagner, G. Eggeler, M.J. Mills, Y. Wang, Acta Mater. 58 (2010) 6685–6694.
[8] J. K-Allafi, A. Dlouhy, G. Eggeler, Acta Mater. 50 (2002) 4255–4274.
[9] J. Michutta, Ch. Somsen, A. Yawny, A. Dlouhy, G. Eggeler, Acta Mater. 54 (2006) 3525–3542.
[10] X. Yao, B. A-Ahmadi, Y. Li, S. Cao, X. Ma, X.-P. Zhang, D. Schryvers, Shape Mem. Superelasticity 2 (2016) 286–297.
[11] O. Bojda, G. Eggeler, A. Dlouhý, Scr. Mater. 53 (2005) 99–104.
[12] K. Kaneko, M. Uehara, H. Aoki, M. Kubo, T. Suzuki, A. Yoshida, J. Soc. Mater. Sci.,

Jpn. 42 (1993) 1103.
[13] M. Elahinia, N.S. Moghaddam, M.T. Andani, A. Amerinatanzi, B.A. Bimber, R.F. Hamilton, Prog. Mater. Sci. 83 (2016) 630–663.
[14] J. Ma, B. Franco, G. Tapia, K. Karayagiz, L. Johnson, J. Liu, R. Arroyave, I. Karaman, A. Elwany, Sci. Rep. 7 (2017) 46707.
[15] J.M. Walker, C. Haberland, M.T. Andani, H.E. Karaca, D. Dean, M. Elahinia, J. Intell. Mater. Syst. Struct. 27 (19) (2016) 2653–2660.
[16] R.F. Hamiltona, B.A. Bimber, M.T. Andani, M. Elahinia, J. Mater. Process. Technol. 250 (2017) 55–64.
[17] S. Saedi, A.S. Turabi, M.T. Andani, C. Haberland, M. Elahinia, H. Karaca, Smart Mater. Struct. 25 (2016) 035005.
[18] M.T. Andani, S. Saedi, A.S. Turabi, M.R. Karamooz, C. Haberland, H.E. Karaca, M. Elahinia, J. Mech. Behav. Biomed. Mater. 68 (2017) 224–231.
[19] S. Saedi, A.S. Turabi, M.T. Andani, C. Haberland, H. Karaca, M. Elahinia, J. Alloys Compd. 677 (2016) 204–210.
[20] S. Saedi, A.S. Turabi, M.T. Andani, N.S. Moghaddam, M. Elahinia, H.E. Karaca, Mater. Sci. Eng. A, 686 (2017) 1–10.
[21] B.A. Bimber, R.F. Hamilton, J. Keist, T.A. Palmer, Mater. Sci. Eng. A, 674 (2016) 125–134.
[22] D.D. Gu, D.H. Dai, G.Q. Zhang, H.Q. Wang, Appl. Phys. Lett. 101 (2012) 171603.
[23] D.D. Gu, C.L. Ma, Appl. Surf. Sci. 441 (2018) 862–870.
[24] K.L. Fukami-Ushiro, D. Mari, D.C. Dunand, Metall. Mater. Trans. A 27A (1996) 183–191.
[25] R. Vaidyanathan, M.A.M. Bourke, D.C. Dunand, Acta Mater. 47 (1999) 3353–3366.
[26] C.L. Ma, D.D. Gu, D.H. Dai, M.J. Xia, H.Y. Chen, CrystEngComm 19 (2017) 1089–1099.
[27] D.D. Gu, B.B. He, Comput. Mater. Sci. 117 (2016) 221–232.
[28] B. Cheng, S. Shrestha, K. Chou, Addit. Manuf. 12 (2016) 240–251.
[29] D. Mari, D.C. Dunand, Metall. Mater. Trans. A 26A (1995) 2833–2847.
[30] D.Y. Li, L.Q. Chen, Acta Mater. 45 (1997) 471–479.
[31] D.Y. Li, L.Q. Chen, Acta Mater. 46 (1998) 639–649.